Supporting Online Information for:

Energy Tracing of Photovoltaic Cells

Yidan An, Tianshu Ma and Xiaofeng Li*

Y. An, T. Ma, and Prof. X. Li
School of Optoelectronic Science and Engineering & Collaborative Innovation Center of Suzhou Nano Science and Technology, Soochow University, Suzhou 215006, China;
Key Lab of Advanced Optical Manufacturing Technologies of Jiangsu Province & Key Lab of Modern Optical Technologies of Education Ministry of China, Soochow University, Suzhou 215006, China.
E-mail: *xfli@suda.edu.cn*

S1. The fundamental energy losses of single-junction SCs

The *pin* heterojunction SC. There are six categories of energy relaxations within the *pin* system, which can be described as follows:[1, 2]

1) *Thermalization*: the photogenerated carriers with energy of $h\nu$ release the excess energy into the material lattice and then relax to the vicinity of bottom of the conduction band ($1.5k_BT + E_c$) or the top of the valence band ($E_v - 1.5k_BT$). The lost carrier energy in this process can be expressed as:[1]

$$H_{therma} = \left(h\nu - E_g - 3k_BT\right) \cdot J_{ph}/q \tag{S1}$$

where $h\nu - E_g - 3k_BT$ is the released excess energy of photogenerated carrier, h the Planck constant, k_B the Boltzmann's constant, T the working temperature of SC, $3k_BT$ the thermal average kinetic energy of carrier,[3] J_{ph} the photogenerated current, and q the charge constant.

2) *Joule heat*: before forming the junction, the *p* and *n*-doping photovoltaic materials have their own quasi-Fermi levels (E_{Fp} and E_{Fn}). When they are brought together, the carrier diffusion leads to the shift of energy bands until their quasi-Fermi levels are aligned under the thermal equilibrium. The built-in potential difference (built-in electric field) is formed due to the energy band shift.[4] Under illumination, the photogenerated minority electrons (holes) will be transported from *p*-doping (*n*-doping) layer to *n*-doping (*p*-doping) layer under the driving force of built-in electric field, leading to the electrostatic potential energy loss of carriers. In the short-circuit situation, the energy losses of carrier in the depletion region can be expressed as:

$$H_{Joule} = \int E \cdot J = \int (-\nabla\varphi/q) \cdot J = V_{bi} \cdot J \tag{S2}$$

where E is the built-in electric field, $\nabla\varphi/q$ the built-in potential difference, V_{bi} the initial built-in potential difference $[V_{bi} = (\varphi_n - \varphi_p)/q = \frac{k_BT}{q}\ln\left(\frac{N_aN_d}{n_i^2}\right)$, φ_n and φ_p the work function of *n* and *p*-semiconductors, respectively,[4] and J the current within the SC.

Under the forward bias, the potential difference will be reduced to $V_{bi} - V$, and thus the Joule heat can be redefined as:

$$H_{Joule} = (V_{bi} - V) \cdot J \tag{S3}$$

Evidently, the Joule heat is closely associated with the initial built-in potential difference, forward bias and the current flowing through the SC junction. Physically, the origin of Joule heat is the reduced carrier potential

energy when the carriers are transported across the depletion region, which is generally regarded as the self-heating effect and therefore it is hard to be removed or even effectively decreased.

3) *Peltier heat at semiconductor-semiconductor (heterojunction) interface*: for the heterojunction device, the heterojunction materials have independent affinities (conduction band) and ionization energies (valance band). When the carriers are transported over the heterojunction interface, the carrier potential energy loss occurs at this interface due to the energy-level offset (conduction and valance band differences are ΔE_c and ΔE_v, respectively).[2] The Peltier heats of electrons and holes at heterojunction interface can be defined respectively as:

$$H_{Peltier\_n}^{SS} = (E_c^i - E_c^n) \cdot J_n/q = \Delta E_c \cdot J_n/q \quad \text{(S4)}$$

$$H_{Peltier\_p}^{SS} = \left(E_v^p - E_v^i\right) \cdot J_p/q = \Delta E_v \cdot J_p/q \quad \text{(S5)}$$

where J_n and J_p are the electron and hole currents transported over the *n*-*i* and *p*-*i* heterojunction interface, respectively. For the *pin* heterojunction SC, the *n*-doping electron transporting layer (ETL) can effectively extract the electrons and block the holes; similarly, the *p*-doping hole transporting layer (HTL) preferentially extracts the holes.[5] Therefore, almost the same order of magnitude of electrons and holes will be transported over the *n*-*i* and *p*-*i* heterojunction interfaces, so that we have $J_n = J_p = J$.

4) *Peltier heat at metal-semiconductor interface*: before the photogenerated carriers being collected by the electrode, the electrons (holes) have to flow from conduction (valance) band to the corresponding quasi-Fermi level, leading to a decreased potential energy. Therefore, the energy losses of electrons and holes at the metal-semiconductor interface can be respectively defined as:[1]

$$H_{Peltier\_n}^{\mathrm{SM}} = (E_c^n + 1.5k_BT - E_{Fn}) \cdot J_n/q \quad \text{(S6)}$$

$$H_{Peltier\_p}^{SM} = (E_{Fp} - E_v^p - 1.5k_BT) \cdot J_p/q \quad \text{(S7)}$$

where J_n and J_p are the electron and hole currents with the conservation relationship of $J_n = J_p = J$.[4]

5) *Bulk recombination loss*: the dark current in a SC is consisted of the typical bulk recombinations [e.g., Shockley-Read-Hall (J_{SRH}), Auger (J_{aug}), and radiation recombination (J_{rad})], which significantly limit the performance of SC. The energy loss by bulk recombination can be expressed as:

$$H_{Rec}^{Bulk} = (E_g + 3k_BT) \cdot (J_{SRH} + J_{aug} + J_{\mathrm{rad}})/q \quad \text{(S8)}$$

6) *Surface recombination loss*: the minority carriers at the surface of SC undergo a recombination process

due to the surface trap or defect (J_{surf}). Therefore, the energy loss by the surface recombination can be defined as:

$$H_{Rec}^{surf} = (E_g + 3k_BT) \cdot J_{surf}/q \quad \text{(S9)}$$

In the *pin* heterojunction SC system, according to the equations (S3)–(S7), the sum of Joule and Peltier losses can be calculated by:

$$H_{Joule} + H_{Peltier}^{\mathrm{SM}} + H_{Peltier}^{SS} = [(E_g + 3k_BT)/q - V] \cdot J \quad \text{(S10)}$$

The *pn* homojunction SC. Comparing for the *pin* heterojunction SC, there is no Peltier heat caused by the energy band offset at the homojunction interface.[2] Therefore, five kinds of carrier thermodynamic losses are obtained in the *pn* homojunction system, that is, the thermalization, Joule, Peltier heat at the metal-semiconductor interface, bulk and surface losses. Thus, the sum of Joule and Peltier heats can be expressed as:

$$H_{Joule} + H_{Peltier}^{\mathrm{SM}} = [(E_g + 3k_BT)/q - V] \cdot J \quad \text{(S11)}$$

The *pn* heterojunction SC. In the photovoltaics system, the electron and hole currents satisfy the condition of electrical neutrality: $J_n + J_p = J$.[4] If the offset of conduction and valance bands are equal ($\Delta E_c = \Delta E_v$), the sum of Joule and Peltier heats can be expressed as:

$$H_{Joule} + H_{Peltier}^{\mathrm{SM}} + H_{Peltier}^{SS} = [\max(E_g^n, E_g^p)/q + 3k_BT/\mathrm{q} - V] \cdot J \quad \text{(S12)}$$

where E_g^n and E_g^p are the bandgap of n and p-doping materials of forming heterojunction, respectively.

S2. The fundamental energy losses of double-junction SCs

For the four-terminal double-junction SC, the electrical connection of sub-cells is independent, therefore, the carrier thermodynamic losses are from the superposition of top and bottom cells. Hence, the sum of Joule and Peltier losses can be defined as:

$$H_{Joule}^{top} + H_{Joule}^{bot} + H_{Peltier}^{SM\_top} + H_{Peltier}^{SM\_bot} + H_{Peltier}^{SS\_top} + H_{Peltier}^{SS\_bot}$$

$$= [(E_g^{top} + 3k_BT)/q - V_{top}] \cdot J_{top} + [(E_g^{bot} + 3k_BT)/q - V_{bot}] \cdot J_{bot} \quad \text{(S13)}$$

where the superscripts and subscripts ‘top’ and ‘bot’ represent the top and bottom cells, respectively.

However, for the two-terminal double-junction SC, the Peltier heats of metal-semiconductor are only generated at metal-electron transporting layer (ETL) interface of top SC ($H_{Peltier\_n}^{SM\_top}$) and metal-hole transporting

layer (HTL) interface of bottom SC ($H_{Peltier\_p}^{SM\_bot}$), respectively. Under the thermal equilibrium conditions, a unified quasi Fermi level can be reached. Moreover, due to the tunneling effect ($H_{Peltier}^{tunneling}$), the carriers accumulated at the tunnel junction sides lead to the energy loss of ΔE (e.g., recombination or tunneling).[6] Thus, the sum of Joule and Peltier losses can be calculated by:

$$H_{Joule}^{top} + H_{Joule}^{bot} + H_{Peltier}^{tunneling} + H_{Peltier}^{SM\_top} + H_{Peltier}^{SM\_bot} + H_{Peltier}^{SS\_top} + H_{Peltier}^{SS\_bot}$$
$$= \left(E_g^{top}/q + E_g^{bot}/q + 3k_BT/q - V\right) \cdot J \quad \text{(S14)}$$

S3. The calculation of photogenerated and recombination currents

Based on the detailed balance theory (SQ limit), we can acquire the current-voltage (*JV*) characteristics of an ideal SC.[7] Besides, relying on the mass action law: $n^2 = n_i^2 e^{qV/k_BT}$, the non-radiative recombination current can be obtained.[8] Thus, the photogenerated, radiation and SRH recombination currents can be respectively defended as:

$$J_{ph} = q\int_0^\infty \alpha(E)\Phi_s(E)\,dE \quad \text{(S15)}$$

$$J_{rad}(V) = qe^{qV/k_BT}\int_0^\infty \alpha(E)\Phi_{BB}(E)\,dE \quad \text{(S16)}$$

$$J_{SRH}(V) = qe^{qV/2k_BT}\gamma_{SRH}n_i d \quad \text{(S17)}$$

$$J(V) = J_{ph} + J_{rad}(0) - J_{rad}(V) - J_{SRH}(V) \quad \text{(S18)}$$

where k_B the Boltzmann constant, T the temperature of SC, $\alpha(E)$ the absorptivity, $\Phi_s(E)$ the radiation spectrum of *AM* 1.5 solar illumination, $\Phi_{BB}(E)$ the blackbody radiation spectrum of SC, γ_{SRH} the SRH recombination rate, n_i the intrinsic carrier density and d the thickness of the SC. In our calculation, we assume that the $\alpha(E) = 1$, $d = 500$ nm, γ_{SRH}=1/5 μs^{-1}, $n_i = \sqrt{N_c N_v \exp(-E_g/k_BT)}$, in which N_c (N_v) the state density of conduction (valance) and the E_g the bandgap of photovoltaic material, where $N_c = N_v = 2\times10^{19}$ cm^{-3}.

For the two-terminal double-junction SC, the current density can be obtained based on the series role of circuit. Thus, the terminal current can be expressed as: $J(V) = J_{top}(V) = J_{bot}(V)$ thus,[9]

$$\left[J_{ph}^{top} - J_{ph}^{bot} - \left(J_{rad}^{top}(0)\cdot e^{-\frac{qV_{\mathrm{top}}}{k_BT}} - J_{rad}^{bot}(0)\cdot e^{-\frac{q\left(V-V_{\mathrm{top}}\right)}{k_BT}}\right)\right] = 0 \quad (19)$$

where V_{top} and V are the forward bias applied on the top sub-cell and two-terminal double-junction SCs, respectively.

S4. The fraction of carrier thermodynamic characteristics for the absorbed solar power

Under illumination, most of the solar power absorbed by SC will be converted into the unwanted heats (e.g., thermalization, Joule, Peltier and recombination losses) and only a small fraction is converted into electricity. From the Figure S1, we can see that about 20 % of absorbed solar power is consumed by the recombination, Joule and Peltier heats within SC, and the remaining is occupied by thermalization and electrical output. Therefore, the wide-bandgap SC shows a higher proportion of electrical output due to the lower thermalization loss.

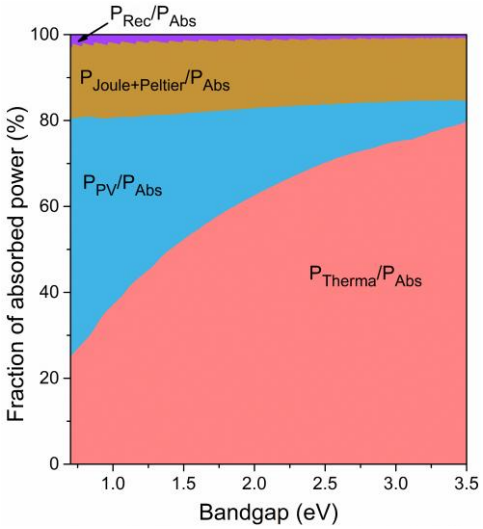

Figure S1. The fraction of various energy conversion processes for the absorbed solar power as the function of bandgap of SC.

The power densities (as well as their fractions) of various energy conversion processes as the fractions of the forward bias for Si and GaAs SCs are shown in Figures S2 (a) and S2 (b), respectively. Similar to the perovskite

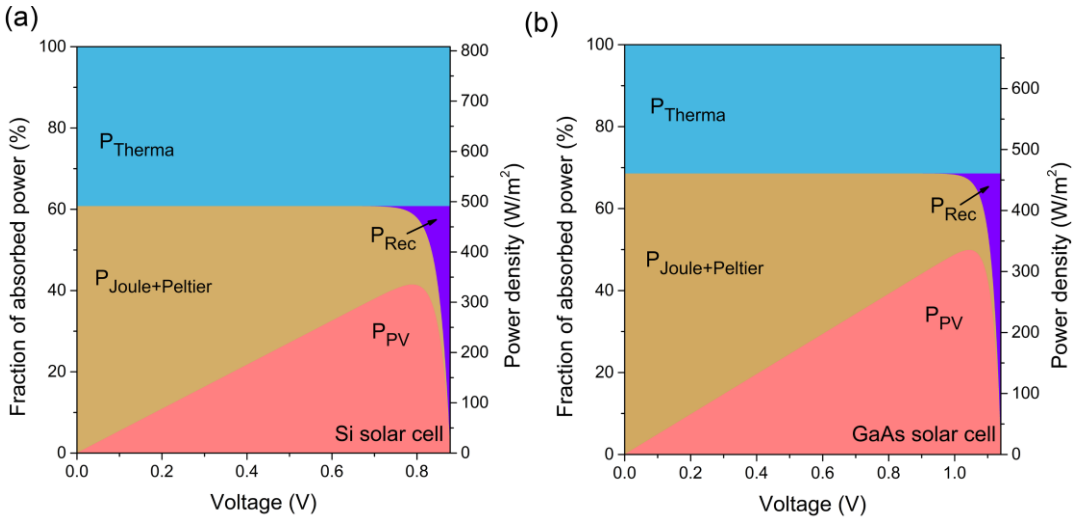

Figure S2. The proportions and power densities of various energy conversion processes as the function of forward

bias for (a) Si and (b) GaAs SCs, respectively.

SC, the thermalization loss is independent of the forward bias. Except for the thermalization, the absorbed solar power is completely consumed by the recombination, Joule and Peltier heats under short-circuit point since there is no electrical output. The Joule and Peltier heats show a significant decline with the increasing bias since the gradually reduced built-in potential. Under the open-circuit point, the recombination will balance with the generation, the absorbed power is consumed by the recombination completely.

S5. The efficiency of practical SC

After considering the SRH recombination (e.g., τ = 5μs, that is the practical SC), the efficiencies of practical SC show a significant decrease comparing for the ideal SC, as shown in Figure S3. It can be seen that the calculated practical efficiencies of typical Si, GaAs and perovskite SCs are 26.3, 27.9 and 26.7 %, respectively. The efficiency of narrow-bandgap SCs show a greatly decrease, which can be attributed to the high intrinsic carrier concentration leading to a higher SRH recombination (see Eq. S17).

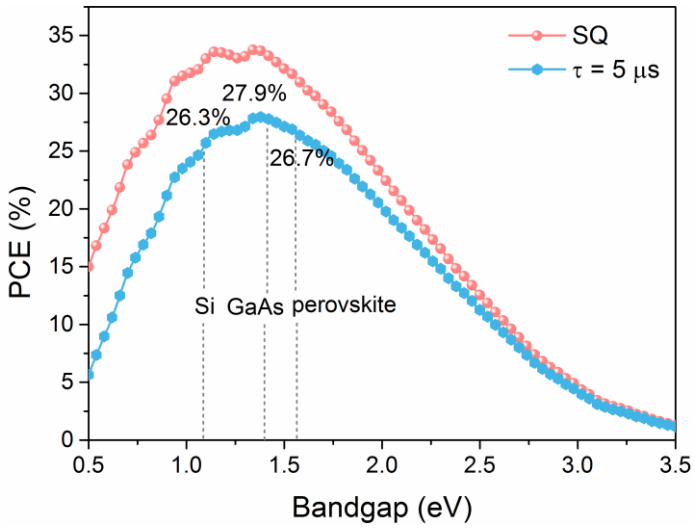

Figure S3. The predicted efficiency of SC as the function of the bandgap of SC, where the carrier lifetime of 5μs is considered in the practical SC.

S6. The operating temperature of double-junction SC systems

The operating temperature of four and two-terminal double-junction SCs are shown in Figures S4(a) and S4(b), respectively. Certainly, a lower operating temperature is obtained in the double-junction SC systems comparing for the single-junction cases. For example, the temperature of single junction Si SC is 57.1 °C, while

those four and two-terminal Si-based double-junction SCs are only 44.69 °C and 44.99 °C, respectively.

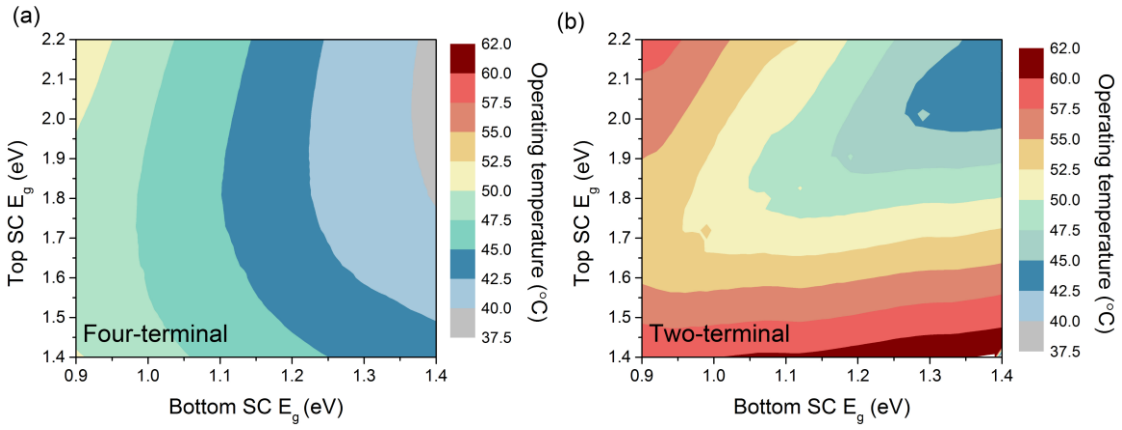

Figure S4. The operating temperatures of the double-junction SCs under (a) four and (b) two-terminal configurations.

References

[1] A. Shang, X. Li. *Adv. Mater*. **2017**, *29*, 1603492.

[2] Y. An, C. Wang, G. Cao, X. Li. *ACS Nano*, **2020**, *14*, 5017.

[3] G. K. Wachutka. *IEEE T. Comput. Aid. D.* **1990**, *9*, 1141.

[4] S. M. Sze, *Physics of semiconductor devices*, John Wiley & Sons, New York, 3rd Ed, **2007**.

[5] Y. An, A. Shang, G. Cao, S. Wu, D. Ma, X. Li. Sol. RRL **2018**, *2*, 1800126.

[6] M. D. Bastiani, A. S. Subbiah, E. Aydin, F. H. Isikgor, T. G. Allen, S. D. Wolf. Mater. Horiz. **2020**, *7*, 2791.

[7] W. Shockley, H. J. Queisser. *J. Appl. Phys.* **1961**, *32*, 510.

[8] L. M. Pazos-Outon, T. P. Xiao, E. Yablonovitch. *J. Phys. Chem. Lett.* **2018**, *9*, 1703.

[9] P. Andreas, P. Pearce, N. J. Ekins-Daukes. *IEEE J. Photovolt.* **2019**, *9*, 679.